GA-C19612

FINAL REPORT
DISPERSED AND PERIODIC MICROSTRUCTURES FOR MAGNETIC AND INFRARED ABSORBERS

by
J.L. KAAE and D.W. DUGGAN

Prepared under
Contract N00014-86-C-0165
for Office of Naval Research
Arlington, VA

MARCH 1989

GENERAL ATOMICS

GA-C19612

FINAL REPORT
DISPERSED AND PERIODIC MICROSTRUCTURES FOR MAGNETIC AND INFRARED ABSORBERS

by
J.L. KAAE and D.W. DUGGAN

Prepared under
Contract N00014-86-C-0165
for Office of Naval Research
Arlington, VA

GENERAL ATOMICS PROJECT 3824
MARCH 1989

1. INTRODUCTION

This is the final report on a study of the electromagnetic characteristics of model materials having a finely divided ferromagnetic phase in a non-metallic matrix. The overall objective of the work was to achieve a theoretical understanding of the physics of microwave and infrared absorption in these materials, but because of lack of funds only fabrication and microstructure and electromagnetic characterization of one material combination made by one process was completed, although a theoretical framework for analytical modeling of the materials was laid out. The process used to fabricate model specimens that were studied was chemical vapor co-deposition, and the material combination studied was a dispersion of cobalt particles in carbon.

In prior work on chemical vapor co-deposition, it was possible to control the particle size of a dispersed phase over a wide range when deposition was carried out in a bed of fluidized particles (1,2). This process was chosen for initial production of the model materials because it promised the production of materials with a range of dispersed particle sizes not possible by other means. (In practice this indeed proved to be true.) Cobalt was selected for the dispersed phase because of its ferromagnetic properties, and carbon was selected for the matrix phase because of its ease of deposition in the chemical vapor process and because by-products of its deposition reaction would not react with cobalt at the high temperatures required for chemical vapor deposition.

If funds had been available for the program as initially planned, other processes would have been used to fabricate other model specimens with cobalt dispersed in different matrix materials such as alumina and mullite, and the theoretical approach would have been used to analyze the electromagnetic and infrared behavior of the model materials.

2. MATERIALS FABRICATION

2.1 Deposition Using Cobalt Iodide

Cobalt-carbon co-deposition has not been carried out previously by chemical vapor deposition in a fluidized bed of particles. The usual method employed to introduce a metal into the coater during chemical vapor deposition is to create a volatile halide and then to reduce this halide with hydrogen. For example, hafnium can be introduced as hafnium chloride where the hafnium chloride is created by passing chlorine gas over heated hafnium metal. Cobalt, however, poses a problem for this method of introduction because the halides of cobalt have high melting temperatures and thus, they have low vapor pressures at moderate temperatures. The only cobalt halide that appears to have a high vapor pressure at temperatures below 1000°C (the data on the vapor pressure of the cobalt halides are limited) is cobalt iodide. Since iodine is a solid at room temperature, the reaction of iodine gas with cobalt metal to create cobalt iodide did not appear to be an attractive route for formation of this halide, and instead cobalt iodide was formed by passing hydrogen iodide over hot cobalt metal. Still, as will be described below, the stability of cobalt iodide presented problems in our chemical vapor deposition apparatus.

The experimental setup for chemical deposition of the two-phase coatings in most of the coating runs is shown schematically in Fig. 1. The cobalt iodide is formed in a secondary furnace directly below the furnace. The cobalt iodide, hydrogen and propylene (C_3H_6), which is the carbon source, are not mixed until just before they enter the coater, and at this point

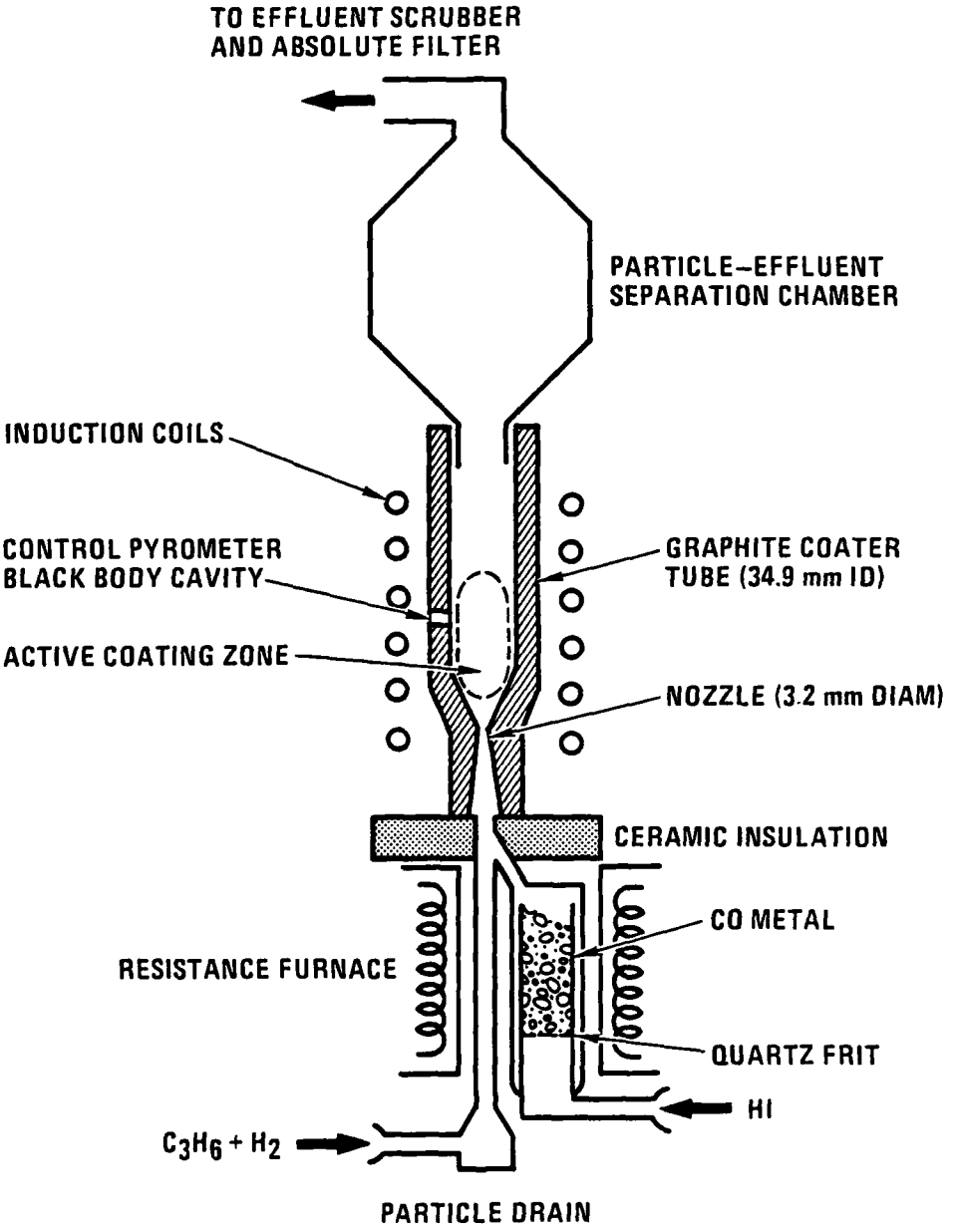

Figure 1: Schematic diagram of the fluidized-bed chemical vapor deposition apparatus setup used for injection of cobalt iodide into the fluidized bed of particles in most of the coating runs.

the gas velocity is high and the temperature is modest so as to prevent reaction of the gases at this position. Instead, the deposition reaction occurs when the gases enter the fluidized bed of particles where the temperature is high. However, the early coating runs were continually shut down by plugging of the system at the point where the gases mixed. The substance that plugged the gas line appeared to be solid cobalt iodide because it was soluble in alcohol. The coating apparatus was altered to increase the temperature at the point in the system where plugging occurred by changing the secondary furnace position, the cooling system at the bottom of the coater and the secondary furnace temperature. Then, reaction to form carbon and cobalt occurred before the gases entered the coater, and plugging of another type occurred. Thus, the stability of cobalt iodide requires a critical control of the temperature before the gases enter the coater in order to prevent the formation of solids in the coater inlet gas lines.

As a partial solution to plugging of the coater inlet lines a wire was introduced that could be rammed up the inlet without shutting the coater down. This allowed operation beyond the times that were possible without the wire, but even with the wire the coater would eventually plug.

The deposition runs that were made in attempts to prepare cobalt-carbon two-phase materials using cobalt iodide as the source gas for cobalt are shown in Table 1. All coating runs were made with the fluidized bed of particles contained in a 34.9 mm ($1\ ^3/_8$ in.) diameter graphite tube; 50 grams of ZrO_2 particles with an average diameter of 500 μm were employed as the particle bed; and, samples for study were obtained by including 9.5 mm

TABLE 1
DEPOSITION CONDITIONS OF THE COBALT-CARBON
TWO-PHASE MATERIALS
USING COBALT IODIDE AS THE COBALT SOURCE GAS

RUN	TEMPERATURE (C)		FLUIDIZING GAS	FLOW (cc/min)		COATING TIME (HRS)	COATING THICKNESS (IN)	Co WT%	COMMENTS
	COATER	COBALT METAL		C_2H_6	HI				
8874-101	1250	750	Argon	1000	100	2.5	0.005	0.2	
8874-103	1250	1000	Argon	500	200	1.5	0.002	3.8	high iodine content in coating
8874-105	1250	1000	Hydrogen	500	400	1.5	0.0004	1.0	low iodine content in coating; selected for examination
8874-107	1293	1000	Hydrogen	500	400	0.4	--	--	
8874-109	1293	1000	Hydrogen	500	400	1.2	0.005	0.02	
8874-111	1300	1000	Hydrogen	500	400	1.5	0.0007	3.5	
8874-113	1350	1000	Hydrogen	500	400	3.0	0.002	10.0	selected for examination
8874-115	1350	980	Hydrogen	500	400	2.5	0.001		
8874-117	1400	980	Hydrogen	500	400	2.5	0.0015		
8874-119	1400	980	Hydrogen	500	400	3.0	0.002		
8874-121	1400	980	Hydrogen	500	400	1.5	0.001		
8874-123	1400	980	Hydrogen	500	400	5.5	0.0032		
8874-125	1400	950	Hydrogen	250	400	4.7	0.0015	1.6	
8874-127	1400	1020	Hydrogen	250	200	1.7	0.0006		
8874-129	1400	1020	Hydrogen	250	200	2.0	0.0007		
8874-131	1400	950	Hydrogen	250	200	1.5	0.0004		
8874-133	1400	875	Hydrogen	250	200	5.5	0.0019	11.0	selected for examination
8874-135	1300	875	Hydrogen	250	200	1.2	--	--	
10004-41	1300	970	Hydrogen	250	200	3.0	0.011	38.4	selected for examination
10004-43	1300	870	Hydrogen	250	200	3.4	0.021	41.0	selected for examination

($^3/_8$ in.) diameter graphite discs in the particle bed. These discs fluidized with the particle bed and were coated with coatings similar to those deposited on the particles.

Coating thicknesses listed in Table 1 were determined by measuring the thicknesses of the discs before and after coating. Cobalt contents were determined by means of energy dispersive x-ray (EDX) analysis in a scanning electron microscope using a piece of pure cobalt as a standard. Iodide contents were determined by the same technique using a no-standard calculational technique. Contents of other trace metals also were determined using the no-standard technique.

Five of the carbon-cobalt materials made by deposition were selected for examination in a magnetometer, and in some cases, transmission electron microscopy was used to characterize the coating microstructure.

Most of the effort on deposition using cobalt iodide was spent in attempts to increase the cobalt content of the deposits while simultaneously overcoming the plugging problem described above.

The first two coating runs (runs nos. 8874-101, 103) were made using argon as the fluidizing gas, assuming that sufficient hydrogen would be present from the decomposition of the propylene to reduce the cobalt iodide. However, a high iodine content was measured in the second of these coatings. To obtain better reduction of the cobalt iodide, hydrogen was

used as the fluidizing gas in the next deposition run, and a low iodine content was achieved. Hydrogen was used as a fluidizing gas in all subsequent deposition runs using cobalt iodide.

There were trace quantities of iron and chromium in many of the coatings made using cobalt iodide. These metals undoubtedly came from the stainless steel container of the cobalt metal and were transported into the coater as iodides.

The cobalt content of the deposit was related to the ratio of the propylene flow to the flow of hydrogen iodide through the cobalt metal. In the range of cobalt metal temperatures used, the cobalt contents of the deposits did not appear to be related to the cobalt metal temperature.

It was thought that reducing the cobalt and carbon flows while keeping the ratio of the two flows constant would not change the cobalt concentration in the carbon but that it might change the size of the cobalt particles distributed in the carbon through a change in the rate of nucleation rate of the particles. The cobalt concentration did remain constant with this change (compare run no. 8874-113 with run no. 8874-133). The cobalt particle sizes of the two samples were not compared by transmission microscopy, but they did behave very differently in a magnetic field. (See Section 3.2)

An entirely different coater setup was used for coating runs 10004-41 and 10004-43. Rather than injecting the cobalt iodide into the main fluidizing gas stream, it was injected into the top of the bed of fluidized particles.

The setup used to do this is shown in Fig. 2. Here the cobalt metal, which was confined in a quartz container, was heated inductively by the same power supply as the fluidized bed of particles, and its temperature was adjusted by adjusting the position of the quartz container in the graphite coater tube.

This latter method of introducing the cobalt iodide into the coater resulted in high cobalt concentrations in the deposit and somewhat alleviated the plugging problem, although it did not entirely eliminate it. (In this setup the cobalt line still eventually plugged.)

The deposits made using this technique were softer than the deposits made using the bottom injection technique. Harder deposits can probably be produced with top injection if the propylene concentration is reduced to lower the coating deposition rate. (Note that these coatings had especially high deposition rates.) Carbon coatings usually become sooty and soft if the deposition rate is to high.

2.1 Deposition Using Cobalt Acetylacetonate

Because of the problem with plugging of the coater inlet when employing cobalt iodide as the cobalt source, we decided to investigate another source gas for the cobalt. The compound chosen was cobalt acetylacetonate, which exists in two forms, Co $(CH_3\text{-}CO\text{-}CH\text{-}CO\text{-}CH_3)_2$ and Co $(CH_3\text{-}CO\text{-}CH\text{-}CO\ CH_3)_3$. The first form known as type II melts at 172°C with no reported boiling point. The second form known as type III melts at 216°C and boils at 340°C. The coater setup for utilizing cobalt acetylacetonate is shown

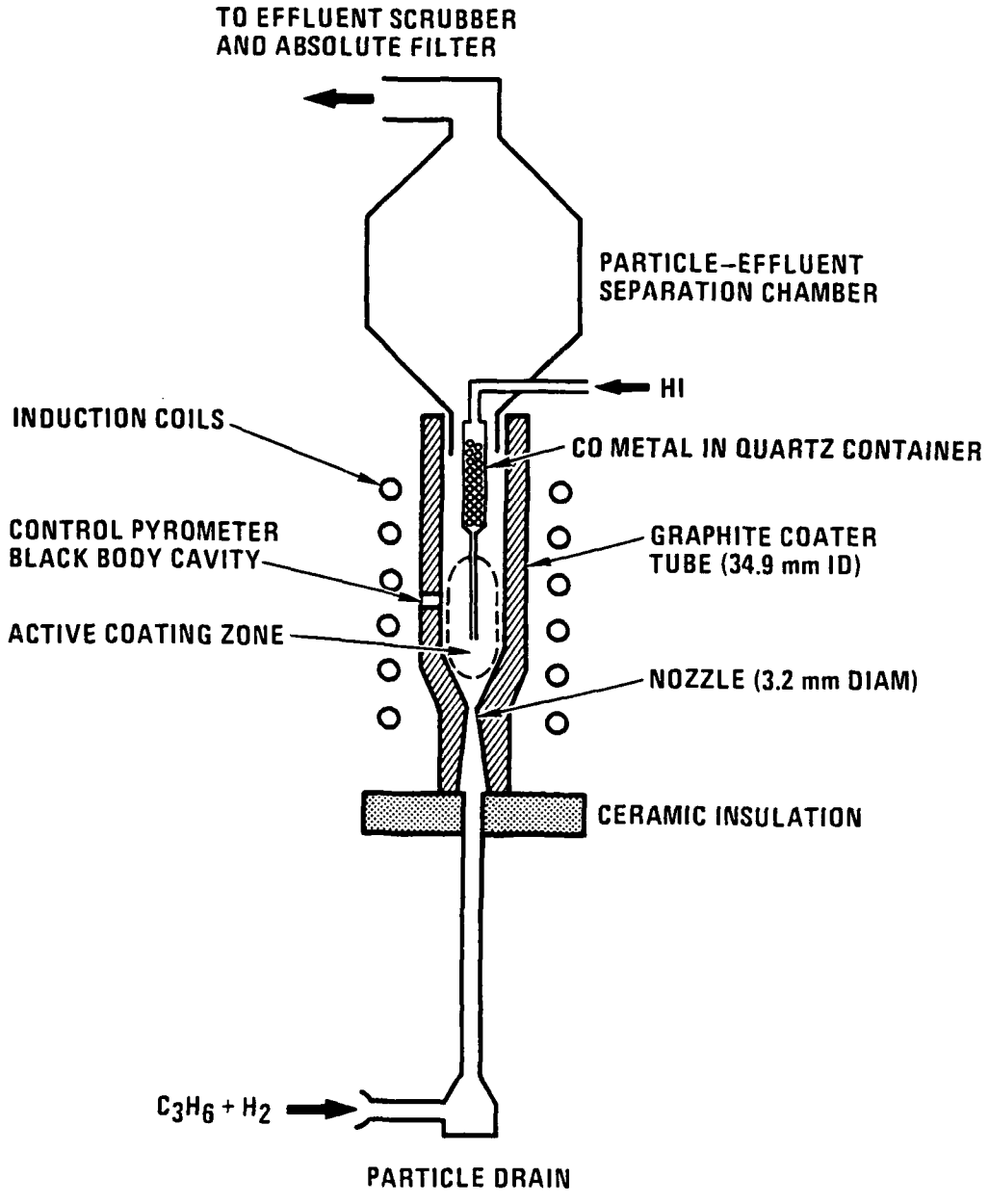

Figure 2: Schematic diagram of the fluidized-bed chemical vapor deposition apparatus setup used for injection of cobalt iodide into the fluidized bed of particles coating runs 10004-41 and 10004-43.

schematically in Fig. 3. In this configuration a carrier gas (either hydrogen or argon) was bubbled through the molten cobalt acetylacetonate, and cobalt acetylacetonate vapor was thereby carried into the coater. The cobalt acetylacetonate was contained in a quartz vessel which as heated in a secondary furnace positioned directly below the main coating furnace. The main carrier gas and the propylene carbon source gas were injected into the gas stream just above the secondary furnace.

The deposition runs made using cobalt acetylacetonate as a cobalt source gas are shown in Table 2. Because of the nature of experimental setup, it was not possible to observe the molten cobalt acetylacetonate as the carrier gas was bubbled through it. However, based on the appearance of the solidified material after deposition runs, the type III cobalt acetylacetonate must have been very viscous in the molten state while the type II cobalt acetylacetonate must have been more fluid. For this reason, more coating runs were carried out with the type II material than with the type III material. The temperature of the type II cobalt acetylacetonate was varied from 215°C to 300°C with both argon and hydrogen as carrier gases and fluidizing gases, but generally very little cobalt was transported to the coating. Because of the low cobalt contents, none of the deposits made in this way were deemed worthy of examination.

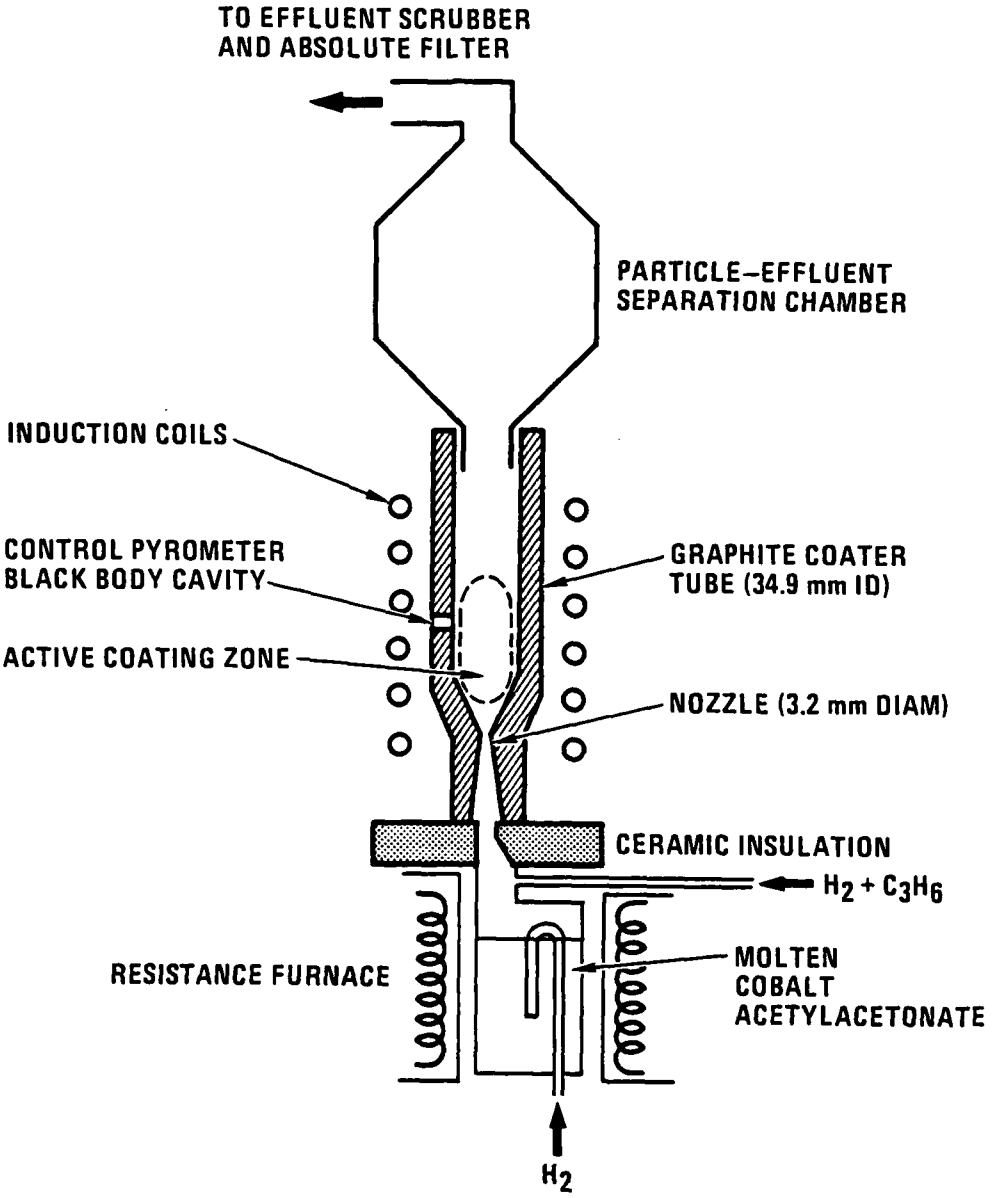

Figure 3: Schematic diagram of the fluidized-bed chemical vapor deposition apparatus setup for injection of cobalt acetylacetonate into the fluidized bed of particles.

TABLE 2
DEPOSITION CONDITIONS OF THE COBALT-CARBON TWO-PHASE
MATERIALS USING COBALT ACETYLACETONATES AS THE COBALT SOURCE GAS

RUN NO.	COBALT ACETYLACETONATE TYPE	FLUIDIZING GAS	TEMPERATURE (°C)		FLOW (cc/min)		COATING TIME (HRS)	COATING THICKNESS (IN)	Co (WT %)
			COATER	ACETYLACETONATE	C_3H_6	ARGON OR H_2 ACETYLACETONATE			
9972-15	III	Argon	1300	260	250	380(A)	5	nil	-
9972-21	III	Argon	1300	260	250	381(A)	1	nil	-
9972-23	III	Argon	1300	260	250	18(A)	0.5	.001	-
9972-25	II	Argon	1300	215	250	18(A)	3	.001	1.6
9972-27	II	Argon	1350	235	500	18(A)	3	.005	nil
9972-29	II	Argon	1350	255	500	18(A)	3	.004	nil
9972-31	II	Argon	1350	275	500	18(A)	5.5	.007	nil
9972-33	II	Argon	1350	300	500	40(A)	4.5	.006	nil
9972-35	II	Hydrogen	1350	300	500	40(A)	2.8	.010	nil
9972-37	II	Hydrogen	1350	300	500	40(H_2)	5.5	.003	nil
9972-39	II	Hydrogen	1350	280	1000	40(H_2)	5.5	.023	nil
9972-41	II	Hydrogen	1350	280	750	40(A)	6.2	.044	nil
9972-43	III	Hydrogen	1350	220	750	40(A)	4.3	.015	nil

3. MATERIAL CHARACTERIZATION

3.1 Transmission Electron Microscopy

Specimens for examination by electron microscopy were obtained by splitting a coated disc and then grinding the soft graphite away from the hard carbon. The resulting thin carbon wafer was then mechanically polished until it was about 0.001 in. thick, after which it was subjected to argon ion bombardment, which sputtered away the carbon-cobalt material, until a small hole appeared. The region around the hole produced in this way was sufficiently thin for transmission by 100 kev electrons.

The electron microscope used to study the microstructure of the carbon-cobalt specimens was a Phillips EM-300. A high-resolution stage, which does not have capability for specimen tilting, was used because the very fine scale of the microstructure required high resolution and because the carbon crystallite size was so small that tilting would have added no additional information. However, the high-resolution stage did preclude the possibility of obtaining multiple electron diffraction patterns from particulate inclusions which would have aided the identification of the cobalt-containing phase.

A transmission electron micrograph of a typical region of a specimen taken from a disc coated in run no. 8874-113 is shown in Fig. 4. The microstructure in the upper left-hand corner of the micrograph is typical

Figure 4. Transmission electron micrograph of coating number 8874-113. The spherical particle marked by the arrow is thought to be a cobalt-containing phase.

of that of pyrolytic carbon with a density of about 1.6 g/cm^3 (3). The spherical black particle in the center of the micrograph is a single crystal, and is presumably the cobalt-containing phase because no such particles occur in pure carbon. Diffraction spots with identical spacings from the center transmitted beam repeatedly occurred in selected area diffraction patterns from regions containing spherical particles. An example is shown in Fig. 5. The planar spacing associated with this diffraction spot is compared in Table 3 with the planar spacings of the hexagonal close-packed form of cobalt which is stable below 420°C, the face-centered cubic form of cobalt which is stable at higher temperatures, or cobalt carbide (Co_2C) which is stable at moderate temperatures. The best agreement of the atomic planar spacing of the spherical particles is with cobalt carbide, but the agreement is not good, and some doubt remains as to the nature of the particles.

The particle shown in Fig. 4 is about 200 Å in diameter. Other particles observed in this sample ranged from about 100 Å to about 400 Å in diameter.

The carbon structure is much coarser in the regions surrounding the spherical particles than elsewhere, and this lends support to the argument that the particles are cobalt carbide. (See for example Fig. 6.) At high temperatures, metal carbide particles are known to migrate through carbon absorbing poorly crystalline carbon on the front surface and precipitating more crystalline carbon or graphite on the back surface. The process is known as catalytic graphitization. The coarse carbon structure near the particles may be evidence that this type of particle migration occurred subsequent to deposition.

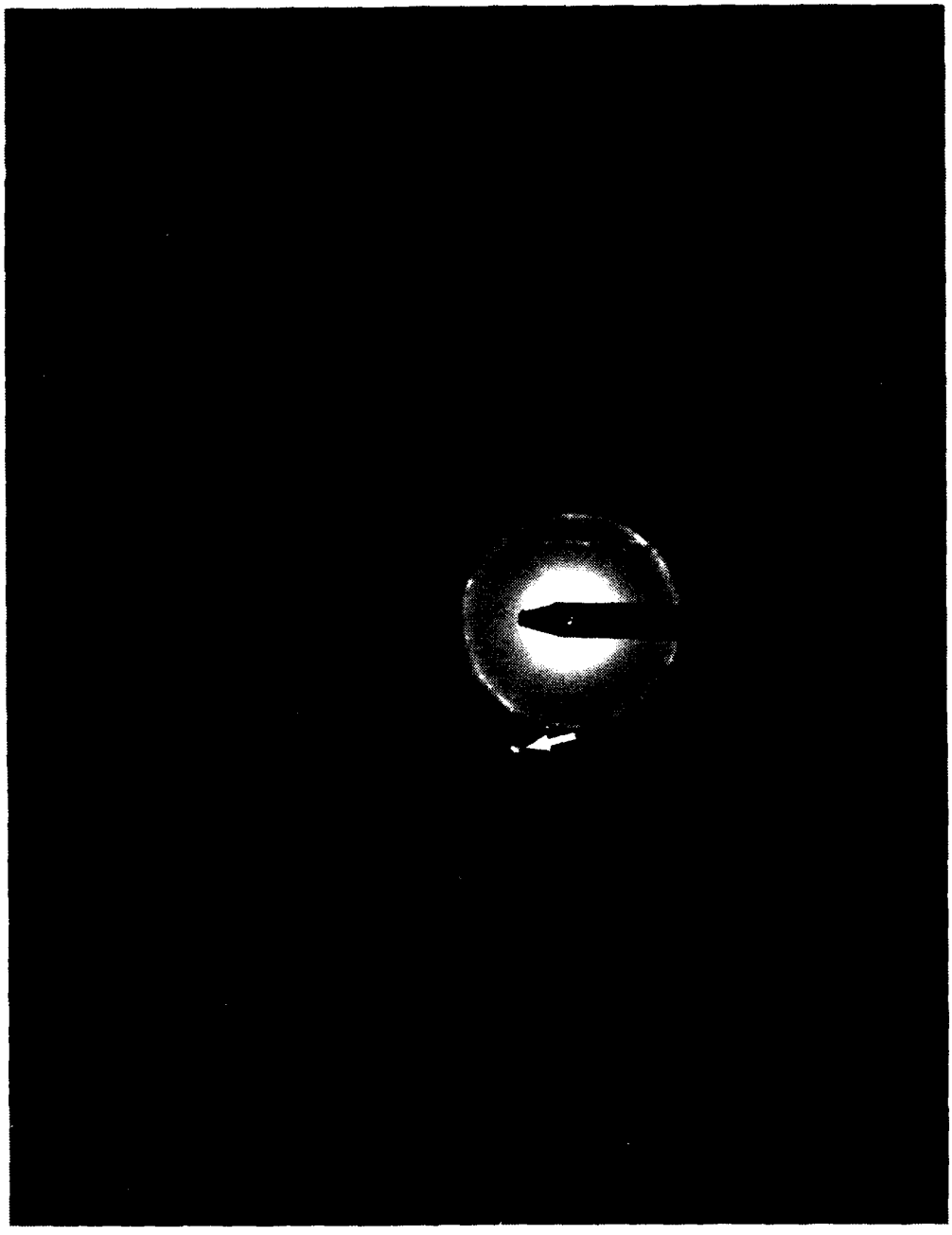

Figure 5. Electron diffraction pattern from the region shown in Fig. 4. The diffraction point marked by the arrow is from the spherical particle.

Table 3

Comparison of Atomic Planar Spacings of HCP Cobalt, FCC Cobalt and Cobalt Carbide with the Observed Planar Spacing of the Spherical Particles

Spherical Particles	HCP Cobalt	FCC Cobalt	Co_2C
2.55 Å	2.165 Å	2.047 Å	2.414 Å
	2.023 Å	1.772 Å	2.329 Å
	1.910 Å	1.253 Å	2.171 Å

Figure 6. Transmission electron micrograph showing a coarsened carbon structure around the spherical particles, which are marked by arrows.

3.2 Magnetic Properties of the Cobalt-Carbon Two-Phase Material

The magnetic properties of the cobalt-carbon two-phase material were measured with a SQUID susceptometer and are summarized in Table 4. The remanence is the magnetization remaining after the sample has been saturated by a large field and then the field is reduced to zero, while the coercive force is the field necessary to reduce the magnetization to zero after saturation. The ratio of the remanent to the saturation magnetization is called the squareness because when this ratio is one the hysteresis loop is square. Since the saturation magnetization per unit mass is an intrinsic property, it is unaffected by particle size so that the squareness is always proportional to the remanence; dividing the remanence by the saturation magnetization is a convenient way to normalize the remanence so that samples with different amounts of cobalt can be compared. For all of the ferromagnetic samples, the weight percentage of elemental cobalt and the ratio of the remanent to the saturation magnetization, or squareness, were measured precisely and the coercive force was at least estimated. For one sample (10004-41), the coercive force was determined precisely.

The curve of the magnetic moment versus temperature at a field of 50,000 Oe for the first sample studied (8894-105) is shown in Fig. 7. The sample was diamagnetic; the susceptibility was negative, and the magnitude was that expected for pure carbon. This is consistent with the cobalt in the sample being in the form of CoI_2, as indicated by the EDX analysis. Cobalt iodine, is not ferromagnetic (4).

Table 4

Magnetic Properties of Cobalt-Carbon Two-Phase Materials

Sample No.	Cobalt Concentration Inferred from Ferromagnetic Behavior (Weight Percent)	(Volume Percent)	Temperature (Kelvin)	Squareness or M_r/M_s	Coercive Force (Oersteds)
8894-105	0	0	-	-	-
8894-113	8.6	2	7	.119	<500
			295	.115	100-280
8894-133	2.6	0.6	297	.058	150-200
10004-41	17* (44)	4.4* (15)	5	.074	150±5
10004-43	50	18	10	.045	100-200
			298	.036	

*Because this sample was probably incompletely stripped, the numbers in parentheses are probably the correct values.

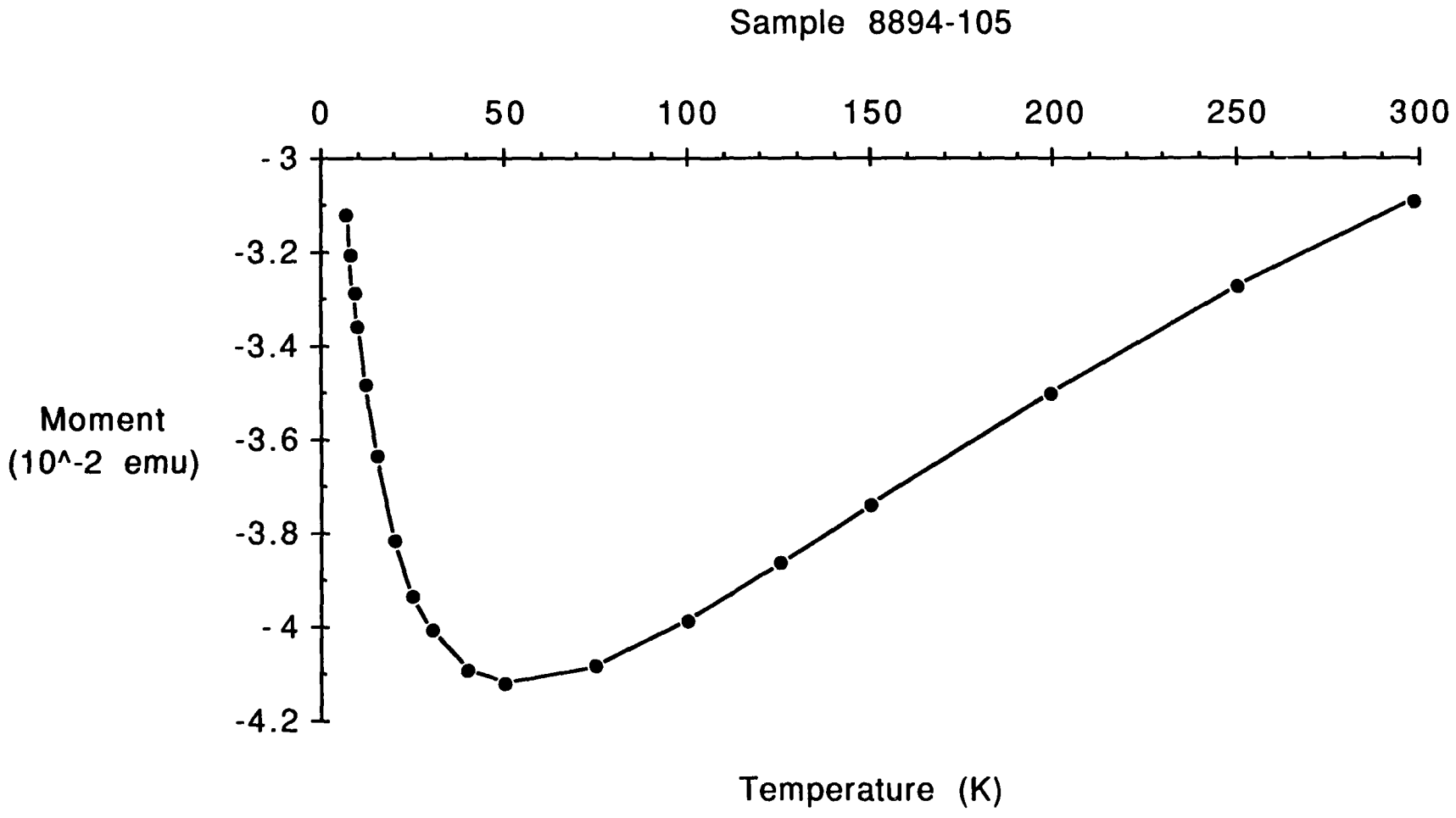

Figure 7. Magnetic moment of sample 8894-105 as a function of temperature at a field of 500,000 Oe.

The curve of the magnetic moment versus the field for the second sample studied (8894-113) in shown in Fig. 8. The saturation magnetization corresponds to 8.6 wt.% Co, assuming that the saturation magnetic moment per gram at 7 K is that of Co at 0 K, namely 162.5 emu/g. This agrees very well with the EDX results. The squareness is about .12 and is only weakly temperature dependent.

The third sample studied (8894-133) contains much less cobalt than the second, only 2.6 wt.%, but the squareness of the loop taken at 297 K, which is shown in Fig. 9, is .058, much lower than the second sample. The coercive force is probably about the same.

The measured cobalt content of the fourth sample studied (10004-41), 17 wt.%, is probably only a lower limit. It actually contained almost as much cobalt, 2.4 mg, as the fifth sample studied, which contained 2.7 mg, but it weighed almost three times as much and was much thicker than any of the other samples. All the samples were coatings deposited on the graphite substrate which was stripped away before the measurements. The fourth sample was probably only partially stripped, and the coating itself probably contains about 10% less cobalt than the fifth sample or about 44 wt.% (15 vol. %). The coercive force was determined very precisely for this sample as shown in Fig. 10. It is 150±5 Oe at 5 K, a value typical of bulk cobalt. The squareness is .074, much lower than in the second sample.

More cobalt, 50 wt.%, was found in the fifth sample studied than in any other. It also had the lowest squareness, only .045 at 10 K, and the squareness was strongly temperature dependent, falling to .036 at 298 K. The coercive force

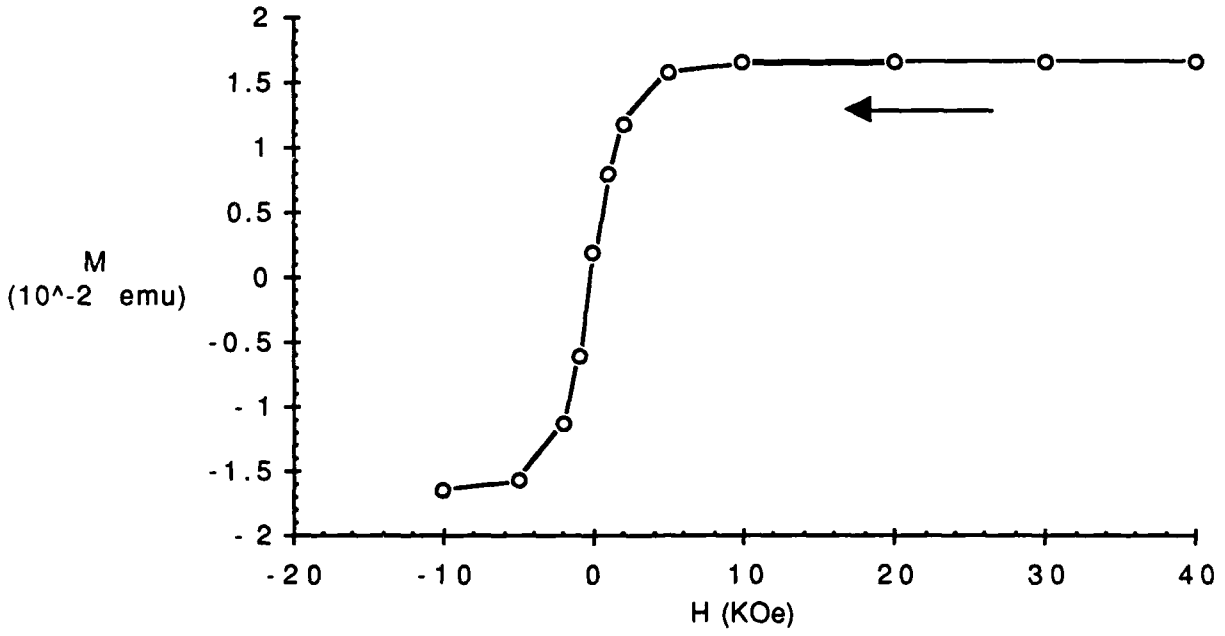

Figure 8. The magnetic moment of sample 8894-113 as a function of the applied field at 297 K.

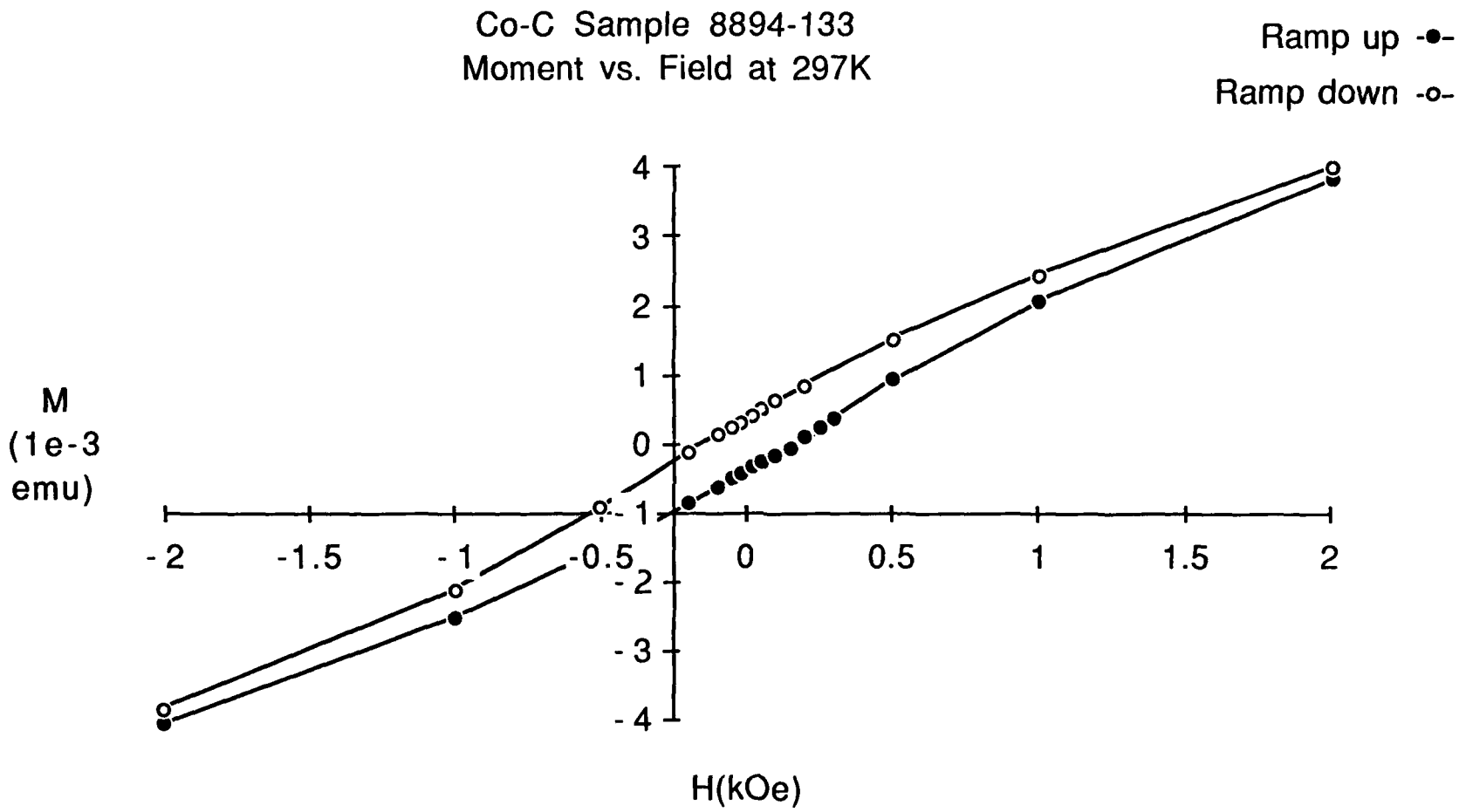

Figure 9A. The magnetic moment of sample 8894-133 as a function of the applied field at 297 K.

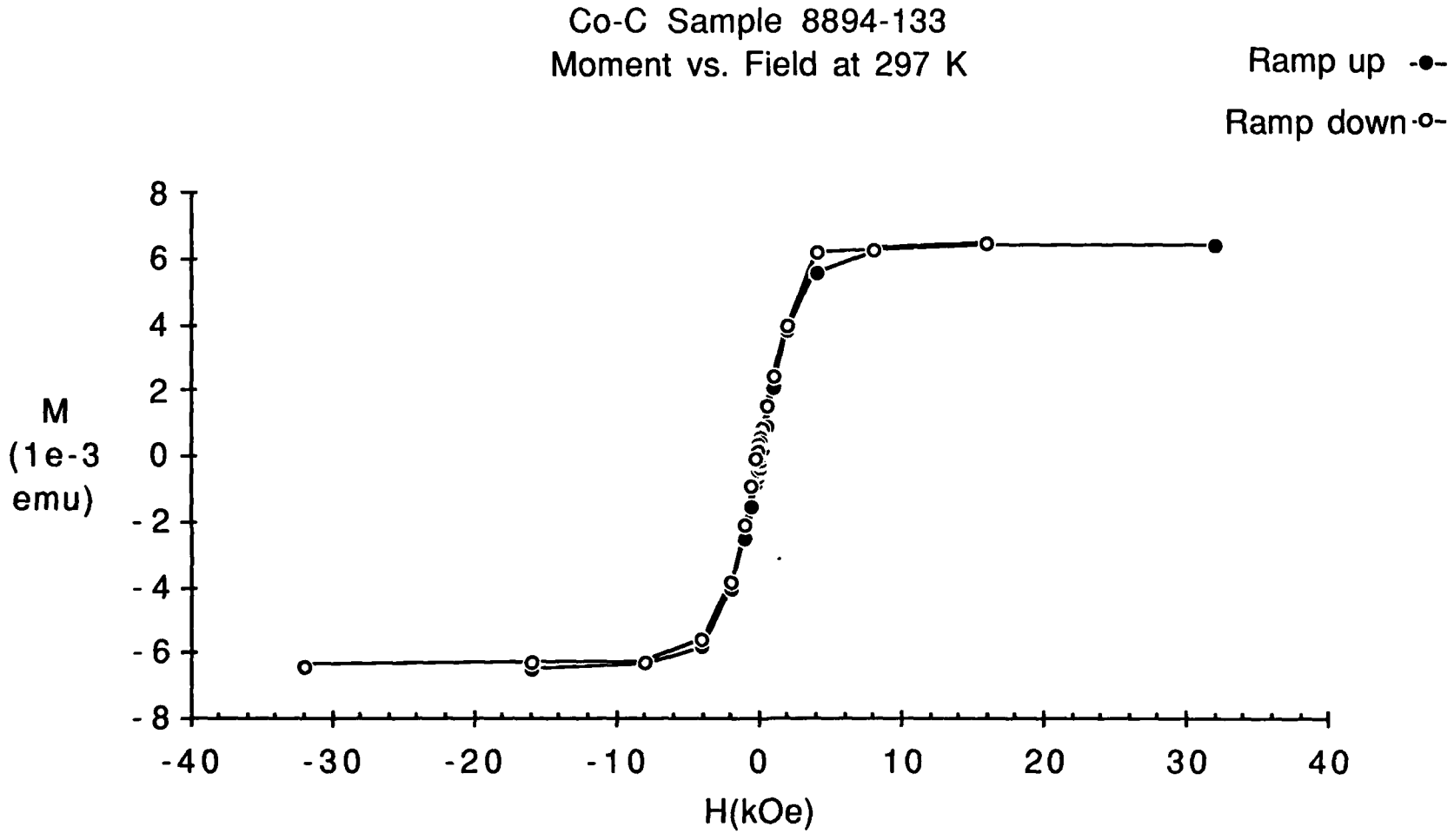

Figure 9B. The magnetic moment of sample 9984-133 as a function of the applied field at 297 K.

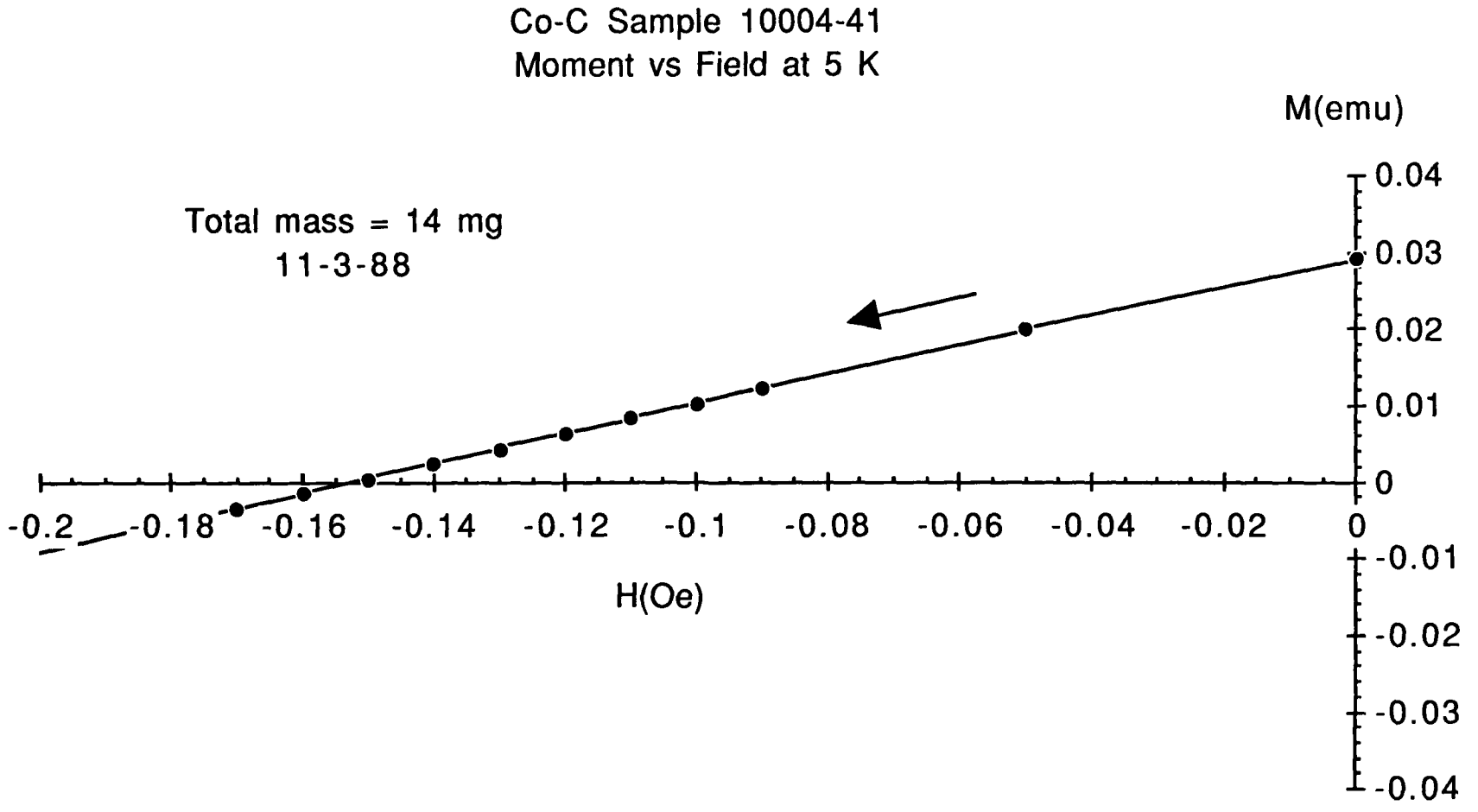

Figure 10. Determination of the coercive force of sample 10004-41.

is probably about the same as in the fourth sample. The hysteresis loop obtained at 10 K is shown in Fig. 11.

The small values of the coercive force and squareness in all the samples would be expected for a mixture of stable single domain particles with either larger multidomain particles or smaller superparamagnetic particles (5). In multidomain particles (on the order of 1000 Å in diameter or larger) in an external field, magnetization reversal begins the same way as in large crystals. Favorably oriented domains, which have lower potential energy, grow at the expense of neighboring domains with higher potential energy. The coercive force in large particles is therefore in the same range as bulk values. However, if a particle is just small enough that it is energetically favorable for it to form a single domain (on the order of 100 Å in diameter) it is very difficult for magnetization reversal to begin, the coercive force can be as high as 1000 Oe, and the remanence also is increased (6). For an assembly of particles, both the remanence and coercive force are lowered from the single particle values by the random orientation of the easy axis of magnetization from one particle to the next.

If a single domain particles is very small (about 40 Å for cobalt at room temperature), its magnetization can fluctuate thermally and its coercive force and remanence vanish. This phenomenon, called superparamagnetism, will occur at a temperature which depends only on the particle size. Thus the coercive force and squareness of an assembly of such particles decrease monotonically with increasing temperature.

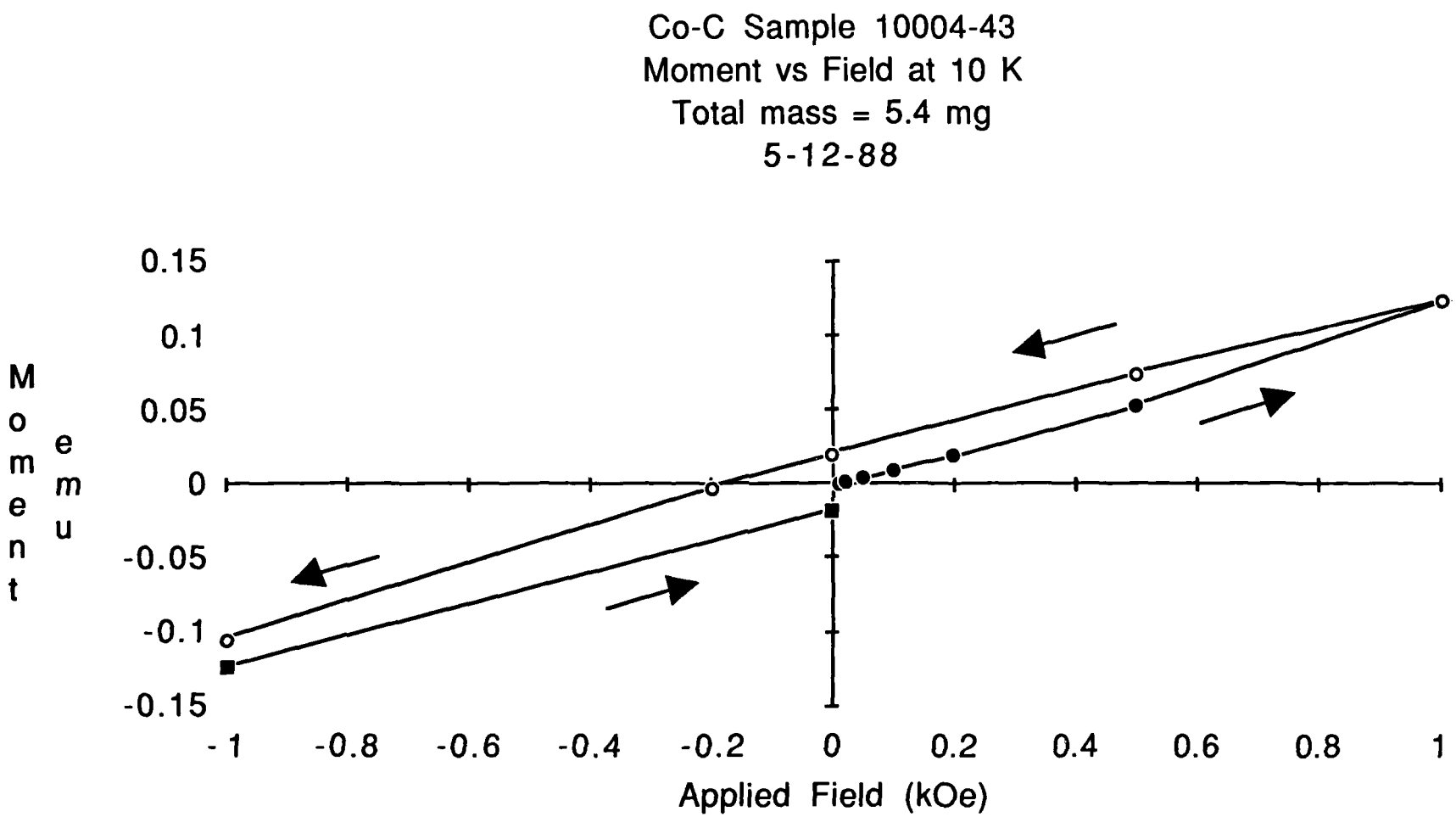

Figure 11. The hysteresis loop of sample 10004-43 at 10 K.

Since the coercive force is the field necessary to reduce the magnetization of all the particles to zero, the coercive force of an assembly of fine particles is the maximum value for any of the particles. The remanence, on the other hand, is the vector sum of the remanent magnetization of all the particles, and the squareness is proportional to the average remanence per spin so that it is essentially a weighted average over the particles with the larger particles weighted more heavily. The squareness would be equal to 0.5 for an assembly of randomly oriented uniaxial particles (7), such as cobalt particles with the hexagonal close packed structure of bulk cobalt, so the small values of the squareness in all the ferromagnetic particles of this study indicate that they contain a large fraction of superparamagnetic particles.

The coercive force appears to be the same in all four of the ferromagnetic samples, indicating the absence of any significant fraction of stable single domain particles. The squareness seems to decrease with metal volume fraction, although sample 8894-133 does not fit the trend. In samples with metal volume fractions over about 10%, interactions between the particles cannot be ignored. One effect of interactions may be to reduce the remanence of the assembly.

4. THEORY

The theoretical effort, has been devoted to establishing a numerical scheme to investigate the interaction effect between microparticles randomly dispersed in a host material. The interaction effect manifests itself in the volume loading fraction dependence of the macroscopic properties of the composite. The standard theoretical treatment of the problem, such as the Maxwell-Garnett theory or the effective medium theory, often invokes the concept of the mean-field in which correlations between (induced) electric or magnetic dipoles are ignored. Different analytic approximations give similar results in the regime of small volume loading fractions of microparticles, but the predictions often deviate significantly from one another in the high volume loading regime. Furthermore, these analytic approaches give no estimate of the local fluctuations of electric polarization or magnetization, which are expected to be important in determining electromagnetic scattering properties of the composite. It is, therefore, of significance to study the problem with a completely different approach.

Our numerical simulation scheme is based on a supercell calculation similar to that of band structure calculations of random alloys. A given number N of microparticles is randomly distributed in a cell of volume L^3. The cell size is chosen to be consistent with the volume loading fraction $f=(4\pi/3a^3N/L^3)$ where a is the radius of the particles. To avoid the finite size effect, we impose a periodic boundary condition. Within the dipole approximation, the internal (electric or magnetic) field acting on the i-th particle,

$$\vec{E}_p(\vec{r}_i) = \sum_{j\neq i} \left\{ \frac{3(\vec{p}_j \cdot \vec{r}_{ij}) r_{ij} - r_{ij}^2 \vec{p}_j}{r_{ij}^5} \right\} = \vec{E}_p(\vec{r}_i; \vec{p}_1, \vec{p}_2, \ldots, \vec{p}_N)$$

or

$$\vec{H}_m(\vec{r}_i) = \sum_{j\neq i} \left\{ \frac{3(\vec{m}_j \cdot \vec{r}_{ij}) \vec{r}_{ij} - r_{ij}^2 \vec{m}_j}{r_{ij}^5} \right\} = \vec{H}_m(\vec{r}_i; \vec{m}_1, \vec{m}_2, \ldots, \vec{m}_N)$$

can be expressed in terms of the Ewald sum. Substituting this equation into the appropriate force equation allows determination of the moments for a given particle distribution in the supercell. For a given number of particles, N, and a given particle configuration a set of 3N X 3N simultaneous equations can be solved. Such a numerical scheme with $N \leq 50$ is well within present-day computer capacity. It should be noted that, in the case of dielectric composites, the familiar Maxwell - Garnett theory is easily obtained by taking N=1.

5. SUMMARY

Model materials for study of the effects of small dispersed ferromagnetic particles on electromagnetic properties have been made by chemical vapor deposition in a bed of fluidized particles. In these materials the continuous phase is carbon and the dispersed phase is cobalt.

To the authors' knowledge, the size of the dispersed cobalt particles, which are spherical with diameters of 100Å to 400Å, is in a range that has not been achieved by other fabrication techniques. Thus, these are unique model materials.

Measurements of the response of these model materials to a magnetic field indicates that the cobalt particles are primarily superparamagnetic and that there is no significant fraction of stable single domain particles

A theoretical framework for investigating interactions between ferromagnetic microparticles has been established. This framework involves the use of supercell calculations.

REFERENCES

1. "The Structure and Mechanical Properties of Co-Deposited Pyrolytic Carbon-Silicon Carbide Alloys", J. L. Kaae and T. D. Gulden, Journal of American Ceramic Society, 54, 605 (1971)

2. "Microstructures of Pyrolytic Carbon-Silicon Carbide Mixtures Co-Deposited in a Bed of Fluidized Particles", J. L. Kaae, Carbon, 13, 51 (1975)

3. "Microstructures of Isotropic Pyrolytic Carbons", J. L. Kaae, Carbon, 13, 55 (1975)

4. American Institute of Physics Handbook, editor Dwight Gray, McGraw Hill, 1963

5. "Particle Size Dependence of Coercivity and Remanence of Single-Domain Particles", E. F. Kneller and F. E. Luborsky, J. Appl. Phys., 34, 656 (1963)

6. E. Kneller in Magnetism and Metallurgy, Vol. 1, editors A. E. Berkowitz and E. F. Kneller, Academic Press, 1969.

7. "Remanence Curves of Cobalt Ferrite Powders Obtained by Fractionation of a Suspension Through a Silica-Gel Column", S. W. Charles, R. Chandrasekhar, K. O'Grady and M. Walker, J. Appl. Phys., 64, 5840 (1988)